JOURNAL OF CATALYSIS 140, 84–102 (1993)

^{27}Al NMR, FT-IR and Ethanol–^{18}O TPD Characterization of Fluorided Alumina

E. C. DeCanio,*,†,[1] J. W. Bruno,† V. P. Nero,* and J. C. Edwards*

*Texaco R & D Department, Beacon, New York 12508; and †Wesleyan University, Middletown, Connecticut 06459

Received June 26, 1992; revised October 8, 1992

A series of F/Al_2O_3 samples (wt% F = 0 to 20) has been studied using a combination of solid-state ^{27}Al NMR, FT-IR, and ethanol–^{18}O TPD techniques. Solid-state ^{27}Al NMR is particularly sensitive to amorphous phases or small crystallites present on the catalyst surface, many of which cannot be detected by XRD. ^{27}Al NMR shows the presence of three types of $AlF_3(H_2O)_n$ species (with n varying between 0 and 3) on fluorided alumina. FT-IR studies of ethanol adsorption show that fluoride blocks the sites required for dissociative chemisorption of ethanol. A similar analysis of adsorbed pyridine shows an increase in the number of Brønsted acid sites with the addition of up to 10 wt% fluoride. However, increasing the fluoride loading to 20 wt% decreases the number of Brønsted acid sites. The TPD of ethanol–^{18}O from F/Al_2O_3 samples shows that at low levels fluoride serves to block Lewis acid sites, but at higher levels its predominant role is to increase the Brønsted acidity of the alumina surface. The pyridine adsorption and TPD experiments show that fluoride strengthens the remaining Lewis acid sites.

INTRODUCTION

New environmental legislation in the United States requiring reformulation of gasoline and diesel fuels is making it necessary to develop better, alternative acid catalysts for alkylation and isomerization reactions, and for hydrotreating catalysts for sulfur and nitrogen removal from refinery streams (*1*). Fluorided alumina has been shown to exhibit increased catalytic activity for acid-catalyzed reactions such as cracking (*2–5*), isomerization (*6, 7*), and polymerization (*8*). Additionally, researchers have been investigating the effect of fluoride on the catalytic activity of reduced and sulfided Mo–Ni(Co)/Al_2O_3 hydrotreating catalysts (*9–11*).

The predominant effect of adding small amounts of fluoride to Al_2O_3 is to increase the number of strong Brønsted acid sites on the alumina (*3, 12, 13*). This increased Brønsted acidity, which is attributed to the through-lattice inductive effect brought about by the electronegativity of fluorine, is believed to be responsible for the higher acid-catalytic activity observed with these types of materials (*3*). In the supported metal catalyst (Ni–Mo/Al_2O_3), the presence of fluoride has been shown to affect the metal dispersion, degree of sulfidization, surface area, and hydrodehydroxylation and hydrodesulfurization activities (*9, 10*). For carbon-supported and carbon-covered-alumina-supported Ni–Mo–F catalysts, the presence of fluoride enhances cracking and hydrogenation reactions (*11*). However, the actual chemistry of the fluoride species and the causes of these effects are not fully understood.

Several techniques have been applied to the study of acid sites on the alumina; these include infrared analysis of adsorbed pyridine, ammonia titrations and amine titrations using H_O and H_R indicators. All these methods provide accurate measurements of the number and strength of the acid sites, but they reveal very little about the structure of the catalyst surface (*14–18*).

Aluminum fluoride formation occurs on

[1] To whom correspondence should be addressed.

0021-9517/93 $5.00

the surface of Al_2O_3 when large amounts of F are incorporated into the Al_2O_3 (*19–22*). There has been little research done to elucidate the relationship between the catalytic activity and the nature of the AlF_3 species, though there is growing evidence that the morphology, and dispersion, of the AlF_3 affects the activity. Early research by Reitsma and Boelhauwer (*23*) suggested that the catalytic sites are located on the crystallite boundary between Al_2O_3 and AlF_3 particles. Moreover, Moerkerken *et al.* (*4*) have shown that Al_2O_3–AlF_3 catalysts containing α-AlF_3 are more active in cumene cracking than are those containing the beta form. And recently, McVicker *et al.* (*19*) have shown that HCF_3-prepared, partially fluorinated Al_2O_3 catalysts maintain higher activites than do conventionally prepared catalysts for isomerization reactions.

In the past, researchers have studied fluorided aluminas using X-ray diffraction (*19, 22, 24*), FT-IR (*13, 20, 21*), XPS (*22*), and ^{19}F NMR (*25*). However, there are contradictory results in the literature concerning the reactions occurring on the alumina surface during the preparation of these samples. Some of these inconsistencies can be attributed to variations in preparation methods; however, most of the inconsistencies involve the XRD technique (which is useful in studying crystalline phases of size greater than 50 Å). It is very possible that some preparations lead to well-dispersed phases that cannot be detected using XRD. We have recently shown that solid-state NMR can be a very useful tool for studying alumina-based catalysts (*26*). In particular, ^{27}Al NMR data reveal the presence of phases that are not detected by XRD.

Recently, we reported the results of a study in which a novel TPD technique was used to investigate the dehydration reactions of ethanol–^{18}O and methanol–^{18}O on γ-alumina (*27*). The TPD experiment is carried out using the probe of the mass spectrometer as the reactor; the proximity of the reactor to the analysis chamber of the mass spectrometer significantly increases the sensitivity of the analysis compared to conventional TPD experiments. We have shown that ^{18}O-labeled alcohols react with Al_2O_3 to form alkoxides via two routes: (1) by dissociative adsorption on Lewis acid sites, giving rise to ^{18}O-containing alkoxide; and (2) by the nucleophilic attack of the surface oxide on alcohol which is probably activated toward C–O cleavage. Furthermore, poisoning experiments using 2,6-dimethylpyridine not only confirmed that the two types of alkoxides form on different alumina sites, but they also showed that adsorption of the pyridine affects the ether desorption temperatures. This suggested that the TPD of ethanol–^{18}O can be used to monitor the changes in the nature of the acid/base sites brought about by the addition of additives to the alumina.

As part of our studies on the role of fluoride in these systems we have carried out an XRD, solid-state ^{27}Al NMR, FT-IR and ethanol–^{18}O TPD investigation of a series of F/Al_2O_3 samples in which the fluorine loading is varied from 2.0 to 20.0 wt%. Our goal is to gain an understanding of the chemistry of the fluoride species on Al_2O_3 supports as a function of loading and pretreatment, and then relate this to the structure of the alumina hydroxyl groups and to the changes in the nature of the acid or base sites on these materials.

EXPERIMENTAL

Sample Preparation

All samples were prepared by the aqueous incipient wetness impregnation technique. Norton 6375C γ-Alumina (20/40 mesh) was impregnated with aqueous solutions of NH_4F (Puratonic grade, Johnson Matthey Inc.) to make the F/Al_2O_3 samples with F loadings of approx. 2, 5, 10 and 20 wt%. The F/Al_2O_3 materials were dried at 110°C for 16 h, and then calcined under flowing air (60 cc/min) for 3 hr at either 200 or 500°C.

The commercial AlF_3 sample used in this study is $AlF_3 \cdot H_2O$ (99.99+% purity grade, Aldrich). To remove the water molecules from the lattice, this material was calcined

under flowing air (60 cc/min) for 3 hr at either 200 or 500°C.

FT-IR Procedure

Infrared spectra were collected using a Nicolet 170 SX FT-IR spectrometer with a liquid-nitrogen-cooled MCT detector. All spectra were recorded after 100 scans with a resolution of 4 cm^{-1}. Spectra were measured using a quartz cell with NaCl windows attached to a glass gas handling/vacuum system. A self-supporting wafer, 1.6 cm in diameter, was prepared by first grinding the sample to 325 mesh size, and then pressing 20 mg of the powder at 6000 psi. The wafers were then mounted in the cell, and evacuated at 5×10^{-5} Torr for 16 h. For the pyridine adsorption experiments, the wafer was dried by heating the sample while under evacuation at 400°C for 2 h, cooled to 100°C, and exposed to 20 Torr pyridine (ultra-high purity grade) for 0.5 h at 100°C. Excess pyridine was removed by evacuating the cell for 1 h at 100°C. The sample was then exposed to 2 Torr of water vapor (ambient temperature) for 2 min at 100°C, then evacuated for 0.5 h at 100°C. FT-IR spectra were recorded at 100°C after this final evacuation step.

The ethanol adsorption experiments were carried out by drying the wafer at 300°C for 2 h while under evacuation, then exposing it to 45 Torr ethanol (absolute ethanol) for 5 min, then evacuating again. The temperature of the evacuated sample was then raised and several FT-IR spectra were recorded at the evacuation temperature.

Solid-State NMR Studies

The solid-state NMR experiments were performed using a Varian Unity-300 spectrometer equipped with full solids capability. The probe was a Doty Scientific 7-mm multinuclear CPMAS probe. The resonance frequency of ^{27}Al was 78.17 MHz, and magic angle spinning rates of 5–7 kHz were employed. The ^{27}Al spectra are referenced to the isotropic MAS resonance of $KAl(SO_4)_2$ (0 ppm). Bloch decay spectra were obtained using ca. 0.6 μs pulsewidth (10° flip angle) and 1 s recycle delays. Cross polarization was employed with an optimized contact time of 0.5 ms, and a recycle delay of 1 s. Aquisition times of 20 ms were used; 4096 data points were accumulated. High-power proton decoupling was employed during aquisition. The ^1H $\pi/2$ pulse used during the cross polarization experiments was 6 μs.

XRD Studies

The X-ray diffraction patterns were collected using a Scintag, PAD IV, $\theta/2\theta$ diffractometer. The diffractometer is equipped with a 2° divergence slit, a 0.3-mm receiving slit, and an intrinsic germanium solid state detector. The samples were ground to a 100 mesh particle size, and top-loaded into the cell. The run conditions used are as follows: power, 45 kV 40 mA: source, Cu $K\alpha$: range, 5°–70° 2θ at 0.03° chopper size at a continuous rate of 0.5° per min.

TPD Procedure

The mass spectrometer was a Finnigan-MAT TSQ70 instrument. The detector was scanned from 12 to 170 Daltons every 0.5 s, and the source was operated at 150°C using a 70-eV ionizing potential with an ion current of 200 uA under electron impact conditions.

Adsorption of the alcohols was achieved by vapor deposition: approximately 0.2 g of alumina was exposed to the vapor of ca. 0.5 ml of the alcohol for 1 h in an air-tight container. Approximately 0.2 mg of each alumina–alcohol sample was placed into a glass insertion tube which was loaded into the temperature-programmed probe of the mass spectrometer and immediately inserted into the source chamber with minimal exposure to air. The pressure of the mass spectrometer source chamber is 1×10^{-7} Torr. The temperature of the sample was increased from 25 to 300°C at a rate of 25°C per min. The probe is within 1 mm of the ionizing electrons, which ensures that the desorbed species are analyzed immediately upon desorption from the alumina surface. This situation minimizes diffusion losses

and time delays and is, therefore, much more sensitive than typical temperature-programmed experiments.

RESULTS AND DISCUSSION

Solid-State ^{27}Al NMR of Aluminum Fluoride

Since AlF_3 formation occurs on the Al_2O_3 surface and plays an important role in the catalytic behavior of fluorided aluminas, we have characterized a commercial sample of AlF_3 (aluminum fluoride hydrate (99.99+%, Aldrich)).

The crystal structure of AlF_3 was determinted by Ketelaar (*28, 29*). AlF_3 forms rhombohedral trigonal trapezohedral crystals in which the metal atoms are 6-coordinate (octahedral) and the fluorides are 2-coordinate (effectively linear). The Al–F, F–F, and Al–Al bond distances are 1.79, 2.53, and 3.51 Å, respectively. The openness of the AlF_3 lattice allows water molecules to be accomodated readily, thereby leading to a range of nonstoichiometric hydrates from which water can be dislodged only with difficulty. Incorporation of water molecules into the lattice causes the lattice arrays to break up, resulting in the destruction of the octahedral symmetry around some of the Al^{3+} ions. Water molecules are then able to occupy coordination sites around these Al^{3+} centers.

The ^{27}Al BD/MAS spectrum of the fresh commercial sample of $AlF_3 \cdot nH_2O$ (Fig. 1A) reveals signals at 40, −10, and −20 ppm. Signals are also apparent at 130 and −100 ppm, but these are spinning side bands. The structure of an AlF_3 crystal, in which the metal ions are 6-coordinate and have octahedral symmetry, should yield one signal in the +30 to −20 ppm range. Solid-state ^{27}Al NMR spectra have been recorded for many aluminum-containing materials, and it has been established that the position of the resonance gives a good indication of the symmetry of the aluminum ion (*30, 31*). The apperance of several signals here reveals that the Al^{3+} ions are in a variety of symmetry environments. Based on literature data

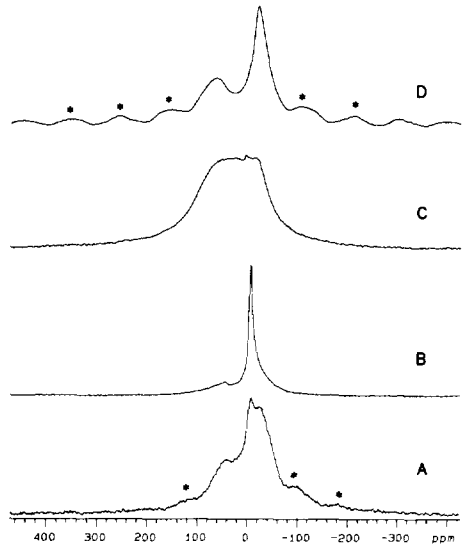

FIG. 1. ^{27}Al BD/MAS NMR spectra of AlF_3 (selective 90° pulse, recycle delay = 1 s, MAS = 5–7 kHz): (A) the fresh sample (NT = 512, LB = 120 Hz); (B) after prolonged exposure to atmospheric moisture (NT = 128, LB = 120 Hz); (C) after a 200°C calcination (NT = 512, LB = 200 Hz); and (D) after a 500°C calcination (NT = 516, LB = 40 Hz). * Denotes spinning side bands.

(*30, 31*), the ^{27}Al NMR resonance at −20 ppm can be assigned to the octahedral AlF_3 species, the −10 ppm resonance to the pseudo-octahedral species in which the Al^{3+} ion is coordinated to three F ions and three water molecules, and the resonance at 40 ppm to a 5-coordinate Al^{3+} species in which two water molecules are bound to an AlF_3 unit (*31*).

The AlF_3 sample was also analyzed after prolonged exposure to atmospheric moisture. The ^{27}Al BD/MAS spectrum of this sample is shown in Fig. 1B. There is a sharp resonance at −10 ppm, which can be assigned to the previously noted $AlF_3(H_2O)_3$ species. Also apparent is the very weak signal at 40 ppm, indicating that another hydrated species is still present. This is in agreement with XRD data that show that this material is in a fully hydrated form, as $AlF_3 \cdot 3H_2O$. Calcining this sample at 200°C gives a material exhibiting the NMR spec-

trum shown in Fig. 1C. It can be seen that this treatment results in the loss of the sharp signal at −10 ppm and the appearance of a broad signal which is the combination of resonances at approximately 40, −10, and −20 ppm. The loss of the sharp signal at −10 ppm shows that some of the water has been removed from the material; however, in agreement with early research (*29*), the NMR data show that there are still significant numbers of water molecules present in the aluminum fluoride lattice. The remaining Al^{3+} ions still occupy sites with different symmetries, and the broad ^{27}Al NMR signal results.

If the AlF_3 is calcined at 500°C, it exhibits one ^{27}Al NMR resonance at −20 ppm and a smaller resonance at ca. 70 ppm (underlying one of the spinning side bands). The spinning side bands are real and are caused by the presence of an Al^{3+} species with a small quadrapole interaction. The resonance at 70 ppm indicates the presence of $AlF_3 \cdot H_2O$. Our XRD data show that this calcination treatment produces the fully dehydrated AlF_3 in addition to a very small amount of hydrated AlF_3. This confirms that the resonance at −20 ppm can be assigned to octahedral Al^{3+} ion which is completely surrounded by six fluoride ions in the lattice.

XRD and Solid-State ^{27}Al NMR of F/Al_2O_3 Samples

A series of F/Al_2O_3 samples (where the wt% F = 2, 5, 10, and 20) have been prepared. The XRD patterns obtained for the calcined F/Al_2O_3 samples are shown in Fig. 2. Fluoride loadings of 2 and 5 wt% give rise to signals at 2θ = 67°, 46°, 39.5°, and 37.5° (the typical diffraction peaks of the gamma alumina support). The presence of 10 wt% F results in additional signals at 2θ = 14.2°, 30.8°, and 32.1°, which are due to the presence of AlF_2OH, and weaker signals at 2θ = 15.8°, 24.8°, and 29.7° due to crystalline AlF_3. These assignments are based on the standard XRD data libraries supplied with the Scintag software. Increasing the F loading to 20 wt% results in the loss of the AlF_2OH diffraction pattern and an increase in the intensities of the AlF_3 diffraction signals. On the $F(20)/Al_2O_3$ sample there is also another phase present as evidenced by signals at 2θ = 17.4°, 24.7° and 28.1°. Based on solid-state NMR data (described later), we can attribute these signals to two hydrated forms of AlF_3, $AlF_3 \cdot 3H_2O$, and $AlF_3 \cdot nH_2O$ (n = 1 or 2).

Previous XRD and XPS studies of F/Al_2O_3 samples have shown that, for F contents over approximately 10 wt%, a $(NH_4)_3AlF_6$ phase is formed inside the pores of the Al_2O_3 surface during impregnation and drying. Upon calcination at successively higher temperatures, $(NH_4)_3AlF_6$ is first transformed into $(NH_4)AlF_4$, and ultimately into α- and β-AlF_3; the overall process is represented in equations 1 to 5 (*20*, *21*). In contrast, Kerkof *et al.* (*32*) were not able to confirm the presence of bulk AlF_3 below F concentrations of 47 wt%; instead they suggested that AlF_2OH forms by exchange of the surface hydroxyl and oxygen atoms with F atoms as shown in Eq. (6).

$$Al^{3+} + 6NH_4F \rightarrow (NH_4)_3AlF_6 + 3NH_3 + 3H^+ \quad (1)$$

$$(NH_4)_3AlF_6 \xrightarrow{170°C} NH_4AlF_3 + 2NH_4F + F^- \quad (2)$$

$$NH_4AlF_3 \xrightarrow{300°C} \text{alpha } AlF_3 + NH_4F \quad (3)$$

$$\text{alpha } AlF_3 \xrightarrow{720°C} \text{beta } AlF_3 \quad (4)$$

$$NH_4F \rightarrow NH_3 + HF \quad (5)$$

$$Al(OH)_3 + HF \rightarrow Al(OH)_2F + HF \rightarrow Al(OH)F_2 + HF \rightarrow AlF_3 \quad (6)$$

In an attempt to characterize the loading process more thoroughly, we have used XRD to study a series of $F(20)/Al_2O_3$ samples which have been subjected to different pretreatment protocols (Fig. 3). The dried sample (Fig. 3A) produces diffraction signals at 2θ = 17.1°, 19.9°, 28.3°, and 34.7°, in addition to the diffraction pattern given by the γ-alumina in the 2θ region 40°–70°. This

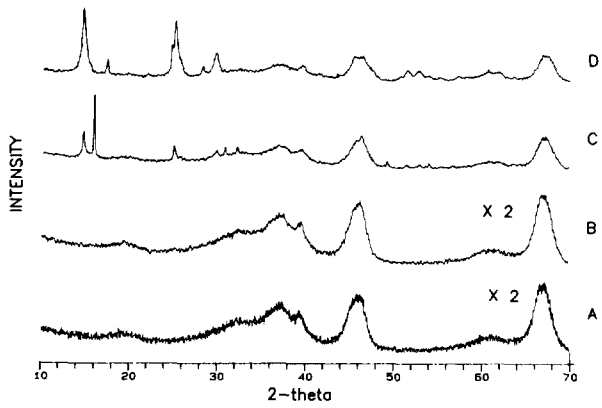

FIG. 2. XRD powder patterns of F/Al_2O_3 (calcined at 500°C) samples: (A) 2 wt% F, (B) 5 wt% F, (C) 10 wt% F, and (D) 20 wt% F.

indicates that the predominant phase on the alumina surface is $(NH_4)_3AlF_6$. Upon calcining the sample at 200°C there is a complete loss of the $(NH_4)_3AlF_6$, and the only diffraction pattern present is that given by the gamma alumina support. This shows that calcining the alumina-supported $(NH_4)_3AlF_6$ transforms it into a dispersed phase not detectable by XRD. As discussed previously, the $F(20)/Al_2O_3$ sample which has been calcined at 500°C yields diffraction patterns due to AlF_3 (2θ = 14.2°, 24.8° and 29.7°), and those of the phase giving signals at 2θ = 17.4°, 24.7°, and 28.14° ($AlF_3 \cdot n(H_2O)$). Hence, our XRD data suggest that AlF_3 can result from both reaction pathways depicted in Eqs. (1)–(6), and the fluoride loading seems to be important in determining which pathway predominates. This is in agreement with Bulgakov and Antipina, who concluded that the ratio of Al_2O_3 to fluoride solution plays a role in determining the type of species formed on the Al_2O_3 (*33*).

We have obtained ^{27}Al BD/MAS spectra for the samples described above, and these are shown in Fig. 4. The spectra were ob-

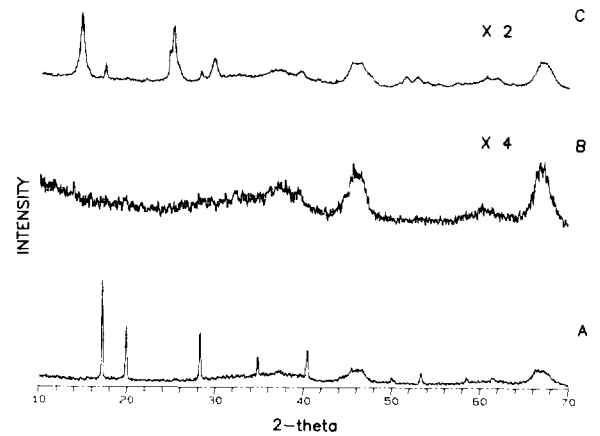

FIG. 3. XRD powder patterns of $F(20)/Al_2O_3$ samples: (A) dried at 100°C, (B) calcined at 200°C, and (C) calcined at 500°C.

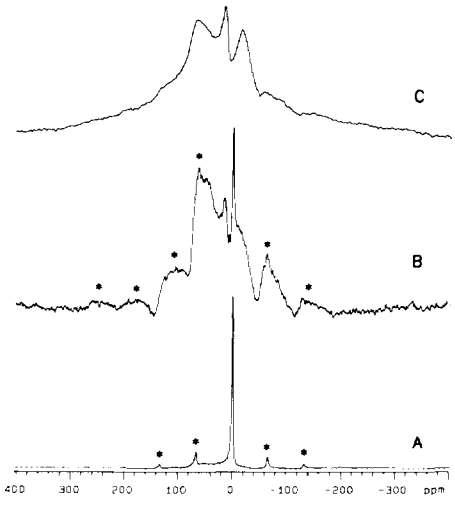

FIG. 4. ^{27}Al BD/MAS NMR spectra of F(20)/Al_2O_3 samples (10° flip angle, recycle delay = 1 s; MAS = 5–7 kHz): (A) dried at 110°C (NT = 512, LB = 100 Hz); (B) calcined at 200°C (NT = 1024, LB = 60 Hz); and (C) calcined at 500°C (Nt = 214, LB = 75 Hz). All spectra have gamma alumina background signal subtracted. * Denotes spinning side bands.

tained by spectrally subtracting the lineshape of the bulk alumina from the F(20)/Al_2O_3 lineshape. All surface Al^{3+} ions that have formed fluoride compounds are observed since the presence of bulk phases on the Al_2O_3 surface precludes any dynamical processes that would give rise to averaged signals (*31*). The dried F(20)/Al_2O_3 sample exhibits a sharp resonance at 0 ppm which can be assigned to the Al^{3+} ions of the $(NH_4)_3AlF_6$. The narrow linewidth of the signal shows that Al^{3+} is in a very symmetrical octahedral environment, consistent with the presence of a crystalline $(NH_4)_3AlF_6$ phase on the alumina surface. Figure 4B shows the spectrum given by the F(20)/Al_2O_3 sample which has been calcined at 200°C. Resonances are observed at −20, 0, 20, and 60 ppm (the remaining signals are due to spinning side bands). The presence of the resonance at 0 ppm shows that some $(NH_4)_3AlF_6$ still remains on the alumina surface; however, it is probably dispersed so that the crystallite size is smaller than the 50 Å necessary for XRD detection. The resonances at −20, 20, and 60 ppm indicate that there are other phases present which are also not detected by XRD. The signal at −20 ppm is most probably due to AlF_3 which has already formed. The signal at 60 ppm appears to be the combination of several resonances. These resonances are probably due to the presence of $(NH_4)AlF_4$ and $AlF_3 \cdot H_2O$ in which the Al^{3+} ions are in tetrahedral environments (*21*). After a 500°C calcination, the F(20)/Al_2O_3 sample gives resonances at −20, 20, and 60 ppm (Fig. 4C). The resonance at 0 ppm has completely disappeared, consistent with the fact that all $(NH_4)_3AlF_6$ has reacted. The resonance at −20 ppm can be assigned to the dehydrated form of AlF_3, while the resonances at 20 and 60 ppm are due to the presence of hydrated forms of AlF_3. The 60-ppm resonance can be assigned to the pseudo-tetrahedral Al^{3+} center of $AlF_3 \cdot H_2O$ and the 5-coordinate $AlF_3 \cdot 2H_2O$ species. The 20-ppm resonance can be attributed to a pseudo-octahedral Al^{3+} center in $AlF_3 \cdot 3H_2O$ (*30, 31*).

Cross polarization (CP) MAS experiments have been carried out on a series of dried F/Al_2O_3 samples. CP/MAS experiments yield information about the Al^{3+} ions which are in close proximity (within 7 Å) to a proton (*34*). The CP/MAS NMR spectrum of dried F(20)/Al_2O_3 has an intense resonance at 0 ppm (Fig. 5A). Upon calcining the F(20)/Al_2O_3 at 200°C, the intensity of the resonance decreases by a factor of 200. The dried F(10)/Al_2O_3 and F(5)/Al_2O_3 samples also exhibit the resonance at 0 ppm (Figs. 5C and D); however, the intensity of the signal decreases with decreasing F loading. In addition to the signal at 0 ppm, the F(5)/Al_2O_3 sample also gives a signal at 10 ppm. The 10-ppm signal is the only feature in the CP/MAS spectrum of dried F(2)/Al_2O_3 and is due to the octahedral site of the alumina surface. The resonance at 0 ppm is again due to $(NH_4)_3AlF_6$. In agreement with our XRD data, this species is present on the dried 10 and 20 wt% samples; however, the NMR data also show that there are still ap-

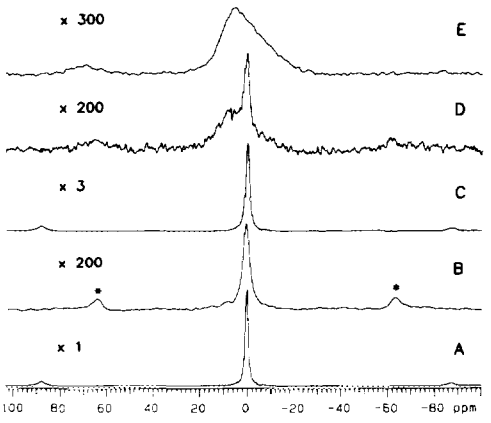

FIG. 5. ^{27}Al CP/MAS NMR spectra of F/Al_2O_3 samples (contact times = 0.5 ms, recycle delay = 1 s, MAS = 5–7 kHz): (A) $F(20)/Al_2O_3$, dried at 110°C (NT = 115); (B) $F(20)/Al_2O_3$, calcined at 200°C (NT = 1504); (C) $F(10)/Al_2O_3$, dried at 110°C (NT = 256); (D) $F(5)/Al_2O_3$, dried at 110°C (NT = 1320); and (E) $F(2)/Al_2O_3$, dried at 110°C (NT = 4289). * Denotes spinning side bands.

preciable amounts present on the $F(20)/Al_2O_3$ sample *after* a 200°C calcination. The appearance of this resonance in the spectrum of the $F(5)/Al_2O_3$ material also shows that $(NH_4)_3AlF_6$ is present at this fluoride loading despite the fact that it is not detected by XRD.

The presence of these phases on the Al_2O_3 surface is reflected in the decrease in both surface areas and pore volumes of the F/Al_2O_3 samples (Table 1). AlF_3 has a low surface area (19) and its formation on the Al_2O_3 surface lowers the overall surface area and blocks the pores of the alumina support.

TABLE 1

Surface Areas and Pore Volumes of F/Al_2O_3 Samples Calcined at 500°C

Sample	Surface area ($m^2\ g^{-1}$)	Pore volume ($cm^3\ g^{-1}$)
Al_2O_3	209.7	1.32
$F(2)/Al_2O_3$	196.3	1.30
$F(5)/Al_2O_3$	184.4	1.29
$F(10)/Al_2O_3$	181.6	1.26
$F(20)/Al_2O_3$	182.1	1.16

IR Studies of the Hydroxyl Region of Dried F/Al_2O_3 Samples

The IR spectra of the hydroxyl region of dried F/Al_2O_3 samples (where the F concentration is varied from 0 to 20 wt%) are shown in Fig. 6. Al_2O_3 exhibits three IR bands at 3569, 3675, and 3725 cm^{-1}. This IR spectrum is typical of a partially dehydroxylated Al_2O_3 surface. The 3569-cm^{-1} band is attributed to the hydroxyl produced by strongly held water (*35*), the 3675-cm^{-1} band is due to the more acidic hydroxyl groups, and the 3725-cm^{-1} band is due to the more basic Al_2O_3 hydroxyl groups (*35, 36*). Incorporation of 5 wt% F into the Al_2O_3 results in the loss of intensity of the 3569- and 3675-cm^{-1} signals. Additionally, there is a shift of the 3725-cm^{-1} band to 3717 cm^{-1}. There appears to be very little change in the IR spectrum when the F loading is increased to 10 wt%. However, increasing the F loading to 20 wt% results in a decrease in the intensities of all the hydroxyl bands. Most notable is the disappearance of the broad signal between 3500 and 3700 cm^{-1}, which is accompanied by the appearance of signals at 3659 and 3555 cm^{-1}.

These IR data show that the addition of fluoride to Al_2O_3 results in the depletion of OH groups on the Al_2O_3 surface, as evidenced by the loss of the signals at 3675 and 3569 cm^{-1}. The presence of the bands at 3717 and 3659 cm^{-1} indicates that only two types of alumina hydroxyl groups remain on the Al_2O_3 surface when high concentrations of F are present. However, the intensities of these bands decrease with increasing F loading, which is consistent with the formation of bulk AlF_3 which covers the Al_2O_3 surface.

Peri (*37*), and others (*13, 20, 24, 32*), have studied the IR spectra of dehydrated Al_2O_3 and F/Al_2O_3 samples. Their data indicate that dehydration causes condensation of the Al–OH groups, producing strained Al–O–Al species as shown in Scheme 1.

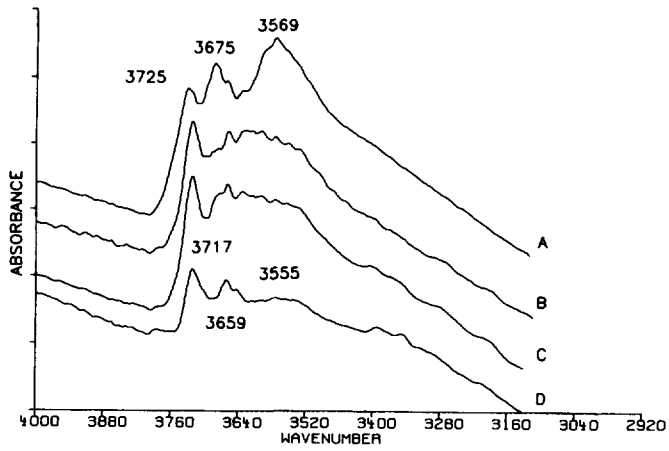

FIG. 6. FT-IR spectra of the hydroxyl region of dried F/Al_2O_3 samples: (A) 0 wt% F, (B) 5 wt% F, (C) 10 wt% F, and (D) 20 wt% F.

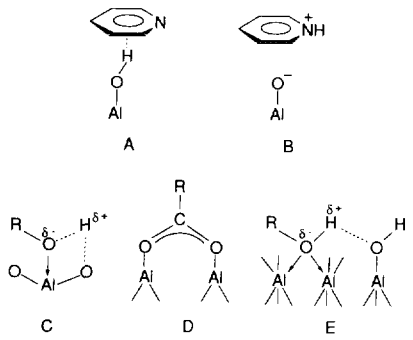

Using CO_2 adsorption and IR analysis, Peri has identified two types of oxides (α and β) with differing reactivites (*38*). He found that at low loadings the fluoride preferentially interacts with the more reactive sites (α sites), but extensive fluoride treatments also eliminate the less reactive (β) sites (*37*). During the calcination, the fluoride ion must react with the Lewis acid center of the strained Al–O–Al species as shown in Scheme 1.

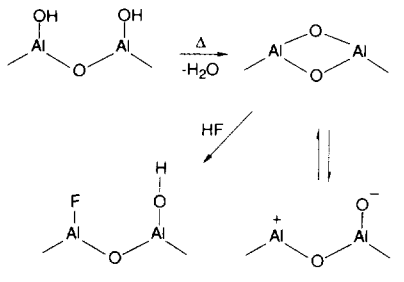

SCHEME 1. Dehydration of Al_2O_3 and the reaction of HF with Al_2O_3.

IR of Pyridine Adsorbed on Dried F/Al_2O_3 Samples

The IR spectra obtained after adsorption of pyridine on the dried F/Al_2O_3 samples are shown in Fig. 7. Pyridine adsorbed on Al_2O_3 (Fig. 7A) exhibits signals at 1452, 1491, 1577, and 1621 cm^{-1} which can be attributed to C–C ring vibrations. Parry established that the band at 1452 cm^{-1} is due to pyridine coordinated to a Lewis acid site (*39*). Pyridine adsorption on $F(5)/Al_2O_3$ produces a new band at 1542 cm^{-1}, and the intensities of all the other bands are greater than those seen for pyridine/Al_2O_3. The band at 1542 cm^{-1} is assigned to the pyridinium ion formed by the interaction between pyridine and a Brønsted acid site (*40*). Increasing the F loading to 10 wt% causes a further increase in the intensities of all the bands (Fig. 7C). However, the intensities of all the IR signals decrease when the F loading is increased to 20 wt% (Fig. 7D). It is known that one of the major effects of incorporating F into Al_2O_3 is to increase the overall acidity

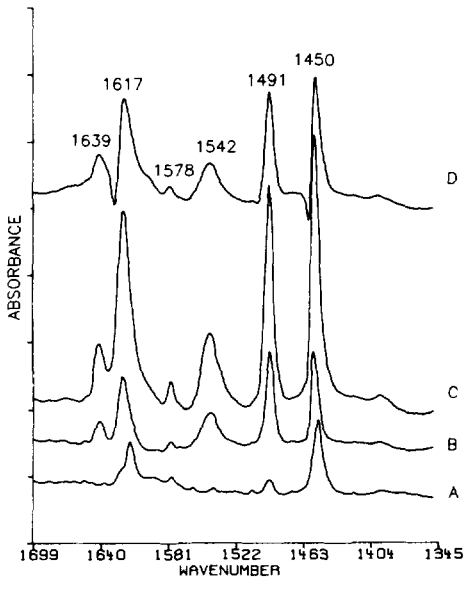

FIG. 7. FT-IR spectra of pyridine adsorbed on dried F/Al_2O_3 samples: (A) 0 wt% F, (B) 5 wt% F, (C) 10 wt% F, and (D) 20 wt% F.

of the Al_2O_3 (*3, 12, 13*). The increase in the strength of the Brønsted acidity is thought to be due to the electronegativity of fluorine, which makes the O–H hydrogens more protonic (*3, 12*). This inductive effect might also be expected to increase the strength of the Lewis acid sites.

Alumina itself exhibits little or no Brønsted acidity, since the Al_2O_3 hydroxyls do not protonate pyridine (Fig. 7A). The incorporation of 5 wt% F in Al_2O_3 creates some Brønsted acid sites, as evidenced by the 1542-cm^{-1} band of protonated pyridine. Increasing the F loading to 10 wt% results in an increase in the intensity of the 1542-cm^{-1} band, showing that the number of Brønsted acid sites are increasing. The increased intensity of the 1452-cm^{-1} band is due to an increase in the overall *strength* of the Lewis acid sites; it has been shown elsewhere that this results because pyridine absorptivities vary with the strength of the Lewis acid site to which the pyridine is bound (*41*). These conclusions are in accord with those resulting from ethanol-^{18}O TPD studies (*vide infra*).

Figure 8 contains difference IR spectra (hydroxyl regions) for pyridine-treated Al_2O_3, $F(10)/Al_2O_3$, and $F(20)/Al_2O_3$; the corresponding spectra obtained before pyridine treatment have been subtracted out. Al_2O_3 exhibits a broad band at 3530 cm^{-1} and very weak negative bands at 3729 and 3762 cm^{-1}. The negative signals are indicative of interactions between alumina hydroxyls and the adsorbed pyridine (*42*). The loss of the 3762-cm^{-1} band may be due to hydrogen bonding interactions between the Al–OH and the pi electrons of the aromatic ring (A) (*42*), while the 3729-cm^{-1} band is due to the formation of a small amount of the pyridinium ion (B) (corresponding to the pyridinium ion observed in Fig. 7). The broad signals at 3530 cm^{-1} are due to the new hydroxyl groups resulting from these interactions. Pyridine on $F(10)/Al_2O_3$ (Fig. 8B) exhibits a very intense negative band at 3724 cm^{-1} and a broad signal in the 3580 to 3500 cm^{-1} region. The intense negative signal at 3724 cm^{-1} is due to the formation of the pyridinium ion (B). Also evident from

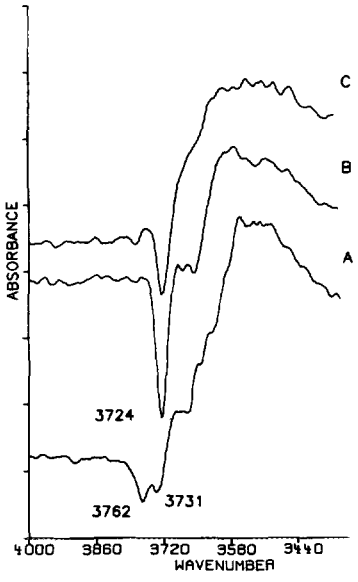

FIG. 8. FT-IR spectra of the hydroxyl region of pyridine adsorbed on dried samples: (A) 0 wt% F, (B) 10 wt% F, and (C) 20 wt% F.

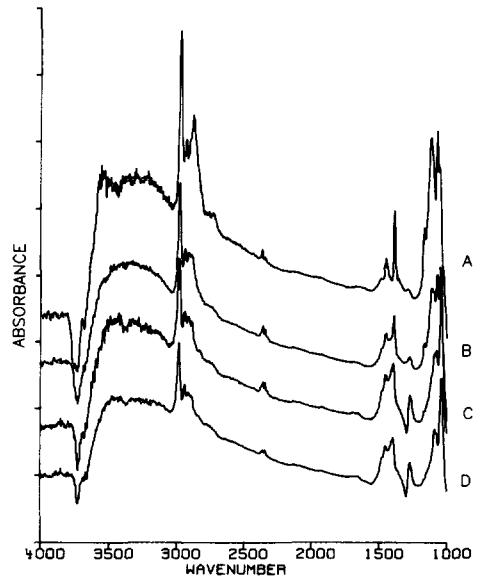

FIG. 9. FT-IR spectra of ethanol adsorbed on dried F/Al_2O_3 samples after evacuating at room temperature: (A) 0 wt% F, (B) 2 wt% F, (C) 5 wt% F, and (D) 10 wt% F.

Fig. 8 is the small shift from 3729 cm^{-1} (for Al_2O_3) to 3724 cm^{-1} (for F/Al_2O_3). This shift is indicative of an increase in the acidic character of the hydroxyl group (*24*). The $F(20)/Al_2O_3$ exhibits the band at 3729 cm^{-1}, but its intensity is lower than that of the $F(10)/Al_2O_3$. This is consistent with the decrease in the density of surface OH groups available for reaction with pyridine.

IR of Ethanol Adsorption on Dried F/Al_2O_3 Samples

Ethanol is often used to study the acid/base chemistry of support materials (*27*). Figure 9 contains the difference IR spectra produced when CH_3CH_2OH (45 Torr, followed by a 5-min evacuation at 1×10^{-5} Torr) is adsorbed onto dried F/Al_2O_3, in which the F loading is varied from 0 to 10 wt%. Ethanol adsorption on Al_2O_3 (Fig. 9A) yields IR bands at 2872, 2930, and 2964 cm^{-1}. The bands at ca. 2964 and 2930 cm^{-1} are assigned to the asymmetric CH_3 and CH_2 stretches, respectively, of the ethyl group. The intense band at 2872 cm^{-1} is assigned to an overlap of the CH_2 and CH_3 symmetric stretches. While the CH_2 symmetric stretch usually falls at 2850 cm^{-1}, the proximity of the C–O group increases the energy of this vibrational mode; it has also been suggested that the *intensity* of the CH_2 symmetric stretching vibration is affected by the proximity of the C–O group (*43*). Also evident in the spectrum are bands at 1447 and 1384 cm^{-1} which are due to the C–H and $C–H_2$ deformations of the ethyl group (*43, 44*).

Additionally, there are several features in the OH stretching region of the spectrum. There is a broad signal centered at 3240 cm^{-1} which can be attributed to the OH bond of the physisorbed ethanol. According to Knözinger and co-workers (*45*), the broad signal centered at 3560 cm^{-1} and the negative signals at 3676, 3728, and 3751 cm^{-1} constitute evidence for the presence of chemisorbed ethanol. From similar data, Knözinger and co-workers (*45, 46*) concluded that there are three types of species produced when short chain alcohols are chemisorbed onto calcined gamma alumina. One such species (C) is produced when the alcohol is chemisorbed onto a coordinatively unsaturated aluminum ion (Lewis acid site). Lateral H-bonding interactions between the alcohol OH group and an adjacent group (such as O^-) contribute to the alcohol OH bond breaking; this species is the precursor state in dissociative chemisorption. The second chemisorption species has a carboxylate structure (D), and is formed only at higher temperatures. The third moiety consists of an alcohol adsorbed onto an acid-base pair site. This site must have an exposed pair of coordinatively unsaturated Al^{3+} ions (an anion vacancy) in the vicinity of a type Ia or Ib hydroxyl group. Type Ia and Ib, etc., are the hydroxyl groups in the model developed by Knözinger to describe the hydroxyl structure of the alumina surface (*34*). In the species depicted in (E) the alcohol is coordinated to a type IIa site in a bridging manner, and the neighboring most basic type Ia group then

offers a lone pair of electrons for interaction with the alcohol proton. The negative signals in the hydroxyl region result from the loss of alumina hydroxyls due to the formation of species E (*46*).

The IR spectrum resulting from the adsorption of ethanol onto F(2)/Al_2O_3 is shown in Fig. 9B. The presence of 2 wt% F causes a small decrease the intensity of all the signals, indicating that there are fewer ethanol molecules being adsorbed onto the Al_2O_3. There are also differences in the nature of the adsorbed species, as evidenced by the difference beween the Al_2O_3 and F(2)/Al_2O_3 spectra in the 2900–3000 cm^{-1} and 1200–1500 cm^{-1} regions. EtOH on Al_2O_3 exhibits intense bands at 2964 and 2872 cm^{-1} and a band of lower intensity at 2930 cm^{-1}, while the analogous F(2)/Al_2O_3 sample produces bands at 2977, 2930, and 2879 cm^{-1}. There is also a notable decrease in intensity of the 2879-cm^{-1} band on the F(2)/Al_2O_3 material.

Lavalley and co-workers have shown that there is a correlation between the position of the C–H stretching bands and the adsorption mode of the alcohol (*47, 48*). When primary or secondary alcohols are dissociatively adsorbed the C–H stretching frequencies are generally shifted to lower values, whereas coordinative adsorption increases the C–H stretching frequencies. The shift toward higher wavenumber of the CH stretch when 2 wt% F is incorporated into the Al_2O_3, therefore, indicates that a greater proportion of the ethanol is coordinatively adsorbed onto the F(2)/Al_2O_3; this may explain the differences (F(2)/Al_2O_3 relative to Al_2O_3) of the intensities of the signals at ca. 2870 cm^{-1}.

The presence of increasing amounts of F on the Al_2O_3 results in a continual decrease in the intensity of the 2879-cm^{-1} band, but does not change the position of the various CH stretching bands. This suggests that added fluoride is causing an overall decrease in the amount of ethanol which is adsorbing on the surface; we attribute this to the build-up of bulk AlF_3, which blocks surface sites.

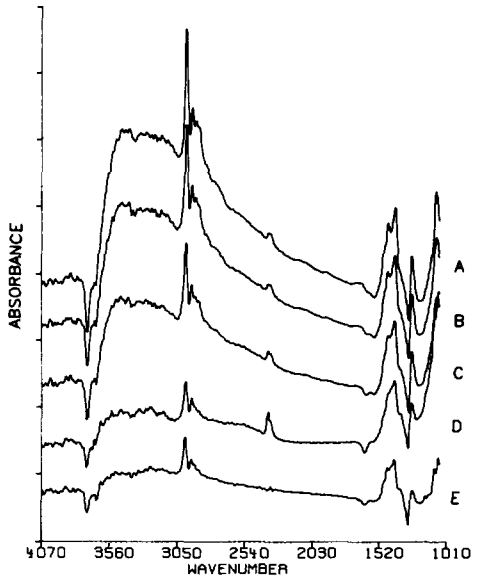

FIG. 10. FT-IR spectra of ethanol adsorbed on F(10)/Al_2O_3 followed by evacuating at: (A) room temperature, (B) 50°C, (C) 100°C, (D) 150°C, and (E) 300°C and cooling to room temperature.

The fact that the presence of 2 or more wt% F on the Al_2O_3 causes a greater proportion of the ethanol molecules to chemisorb in a coordinative fashion is probably due to a reaction of fluoride with the Lewis acid sites; specifically, fluoride serves to block those Lewis acid sites that are required for dissociative adsorption.

Evacuation of the F(10)/Al_2O_3 sample at temperatures up to 150°C (Fig. 10) results in a decrease in the intensities of all the bands, showing that alkoxide species are being desorbed from the catalyst surface. However, after evacuation at 150°C (Fig. 10C) there is still a broad band present at 3420 cm^{-1}. This band is due to the stretch of the OH group of an intact ethanol molecule, indicating that some associatively adsorbed ethanol molecules are still present on the alumina surface. These intact ethanol molecules are not physisorbed species since physisorbed ethanol has been shown to desorb from Al_2O_3 by 50°C (*27*). Evacuation at 300°C, and subsequent cooling to room temperature results

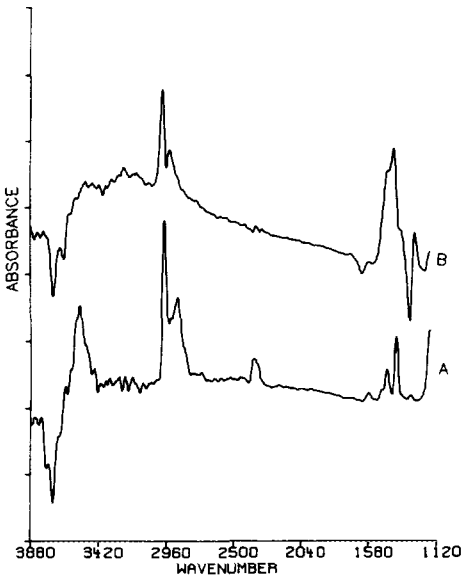

FIG. 11. FT-IR spectra of ethanol adsorbed on samples followed by evacuating at 300°C and cooling to room temperature: (A) Al_2O_3 and (B) $F(10)/Al_2O_3$.

in a large decrease in the intensities of all the signals (Fig. 10E). This decrease is due to the depletion of alkoxide species on the alumina surface, although the signals in the 2800–2900 and 1000–1500 cm^{-1} regions of this spectrum indicate that some remain. Also, the presence of the signal at 3420 cm^{-1} shows that some intact ethanol species remain on the Al_2O_3 surface. A comparison of the IR spectra of Al_2O_3 and $F(10)/Al_2O_3$ samples after the heat treatment (Fig. 11) shows that the signal is not present for Al_2O_3. The presence of intact ethanol molecules on the $F(10)/Al_2O_3$ is indicative of the presence of strongly coordinatively chemisorbed ethanol. Both Lavalley *et al.* (*47*) and Knözinger and co-workers (*45*) have shown that species E can be formed irreversibly at a suitable acid–base site. This suggests that the presence of fluoride on the Al_2O_3 is leading to the creation of acid-base sites upon which ethanol can coordinatively chemisorb in an irreversible fashion.

Thus, FT-IR analysis of ethanol adsorbed on F/Al_2O_3 shows that the addition of fluoride alters the relative amounts of dissociatively and coordinatively adsorbed ethanol; our IR data show that the presence of fluoride promotes the coordinative chemisorption of the ethanol. Furthermore, these coordinatively adsorbed ethanol species are strongly held on the fluorided alumina surface, as evidenced by the observation that an ethanol OH stretching band is present even after evacuation at 300°C. These phenomena are due to the fact that fluoride reacts with sites on the Al_2O_3 surface which are important for dissociative adsorption. In addition, the through-lattice inductive effect of the electronegative fluorine might also be changing the nature of the acid-base sites. Finally, the addition of greater amounts of fluoride results in the decrease in the amount of ethanol adsorbed on the catalyst surface, because surface Al–F and bulk AlF_3 species are formed which block surface sites.

TPD Analysis Using Ethanol–^{18}O

Previously we have shown that ethanol reacts with Al_2O_3 to form alkoxides via the two routes shown in Scheme 2 (*27*). These involve dissociative adsorption on Lewis acid sites, and nucleophilic attack by the surface oxide on an alcohol (which is probably activated toward C–O cleavage). Evidence for this comes from TPD experiments on ethanol–^{18}O adsorbed on gamma Al_2O_3, in which ethylene (m/z = 26, 28) and two ether dehydration products $R^{16}OR$ (m/z = 59, 74) and $R^{18}OR$ (m/z = 61, 76) are observed. Ether formation is the result of the bimolecular reaction between two alkoxides, while the ethylene is the product of the unimolecular dehydration reaction (*27*). It was found that there was no scrambling of the alkoxide sites over a period of 1 week at room temperature, and studies involving 2,6-dimethylpyridine confirm that the alkoxides are formed on different types of sites. Additionally, the materials poisoned with 2,6-dimethylpyridine generate ethers and alkene at higher temperatures than do the nonpoisoned samples.

Ethanol–^{18}O TPD experiments have been

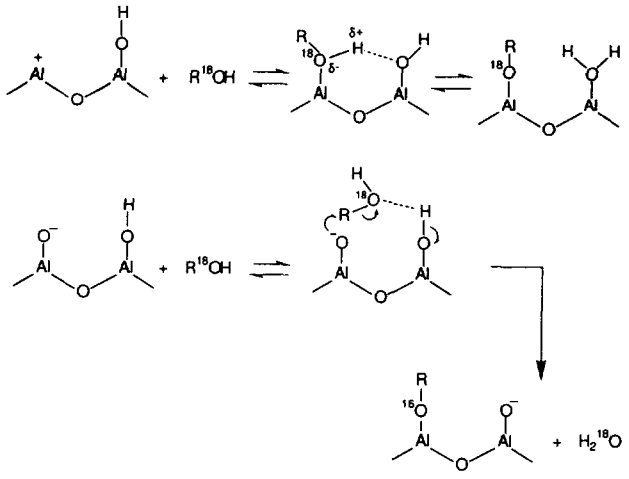

SCHEME 2. Two routes to alkoxide formation on the alumina surface (27).

carried out on a series of F/Al_2O_3 samples (where the F loading is varied from 0 to 10 wt%) in order to understand how fluoride affects the surface acid/base chemistry of the Al_2O_3. The technique employed allows us to perform the TPD experiment any number of times after the vapor deposition. For most of these samples this analysis was performed 1 h, 4 h, and 1 week after exposure to the ethanol–^{18}O. For the sake of clarity, we shall first discuss the TPD results obtained 1 h after the vapor deposition step for each F loading. This will be followed by a discussion of the TPD results obtained as a function of time after the vapor deposition.

A. TPD results as a function of fluoride loading. The partial ion chromatograms for the desorption of ethanol–^{18}O from Al_2O_3 have been published (27). Comparable mass spectral data obtained upon thermal desorption of ethoxides from $F(2)/Al_2O_3$ are shown in Fig. 12, and the detection of $R^{16}OR$ (m/z = 59, 74), $R^{18}OR$ (m/z = 61, 76), ethylene (m/z = 26, 28), and $H_2{}^{18}O$ (m/z = 19, 20) is apparent. Similar data for $F(5)/Al_2O_3$ are shown in Fig. 13. Peak temperatures and the integrated peak areas for the dehydration products are presented in Table 2, and the ratios of the various dehydration products have been calculated in Table 3. It is clear from these data that there is indeed an effect due to added fluoride, but this could result from either (a) differences in the overall population of the surface alkoxides (which was indicated by the IR studies), or (b) differences in the nature of the sites and, hence, in the subsequent elimination reactions. That the latter is at least a contributing factor is indicated by the desorption tempera-

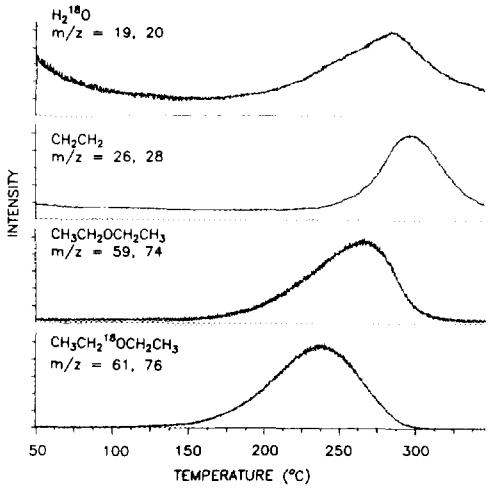

FIG. 12. Reconstructed partial chromatograms of the temperature-programmed desorption products of ethanol–^{18}O adsorbed for 1 h on $F(2)/Al_2O_3$.

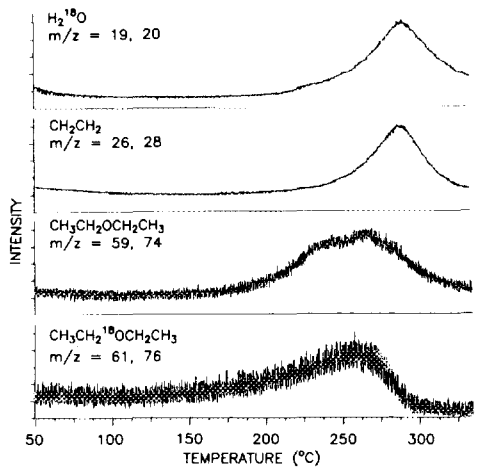

FIG. 13. Reconstructed partial chromatograms of the temperature-programmed desorption products of ethanol-^{18}O adsorbed for 1 h on $F(5)/Al_2O_3$.

tures noted in Table 2; the alkene and ether desorption temperatures both increase substantially upon the addition of 2 wt% fluoride, then level off at higher fluoride loadings. While ether formation requires two proximal alkoxides and should therefore be sensitive to surface population effects, the formation of alkene requires but one alkoxide. The observed dependence of alkene desorption temperatures on fluoride loading confirms that there is a fundamental change in the nature (and *not* just the number) of the alkoxide sites upon the addition of fluoride; we consider the mechanism by which fluoride affects alkene formation below.

The data in Table 3 indicate that the ratio $R^{18}OR/R^{16}OR$ decreases with added fluoride to the level of 5 wt%, then increases with added fluoride up to 10 wt% fluoride. This

TABLE 2

Summary of Peak Temperature and Area for the Dehydration Products of Ethanol-^{18}O Adsorbed on F/Al_2O_3 Samples

F Loading	Product	Peak temp. (°C)	Peak area
0.0	C=C	261	3.42×10^8
	$R^{16}OR$	220	4.95×10^6
	$R^{18}OR$	179	1.59×10^7
2.0			
1 h	C=C	295	1.20×10^9
	$R^{16}OR$	266	2.08×10^7
	$R^{18}OR$	240	6.10×10^7
1 week	C=C	291	8.69×10^7
	$R^{16}OR$	269	2.97×10^6
	$R^{18}OR$	241	9.23×10^6
5.0			
1 h	C=C	285	4.70×10^8
	$R^{16}OR$	237 and 269	5.49×10^6
	$R^{18}OR$	256	1.78×10^6
4 h	C=C	291	4.20×10^8
	$R^{16}OR$	219, 237, and 287	7.05×10^6
	$R^{18}OR$	270	1.69×10^6
1 week	C=C	282	7.67×10^7
	$R^{16}OR$	—	—
	$R^{18}OR$	263	9.90×10^5
10.0			
1 h	C=C	287	4.18×10^8
	$R^{16}OR$	280	1.46×10^6
	$R^{18}OR$	250	3.51×10^6
1 week	C=C	296	1.34×10^8
	$R^{16}OR$	—	—
	$R^{18}OR$	261	3.94×10^6

TABLE 3

Summary of Ratios of Dehydration Products of Ethanol-^{18}O Adsorbed on F/Al_2O_3 Samples

F Loading	$R^{16}OR : R^{18}OR$	$C{=}C : R^{16}OR$	$C{=}C : R^{18}OR$
0.0	0.312	69.0	21.5
2.0			
1 h	0.345	57.8	197
1 week	0.323	29.4	9.43
5.0			
1 h	3.13	85.5	265
4 h	4.17	59.5	249
1 week			77.5
10.0			
1 h	0.417	286	119
1 week			34.0

behavior is highly suggestive of the operation of two (or more) competing effects. We have proposed (*27*) that the ^{18}O-alkoxides arise from the interaction of alcohol with Lewis acid sites on alumina, and we now suggest that the primary effect of fluoride at low loading levels is to block these Lewis acid sites by forming surface Al–F bonds. At higher fluoride levels, the $R^{18}OR/R^{16}OR$ ratio increases, but the integrated peak areas suggest that this is due primarily to a decrease in $R^{16}OR$ production rather than to an increase in $R^{18}OR$ production. We've shown that the ^{16}O-alkoxides are derived from sites that were initially nucleophilic (*27*), and it is reasonable to expect them to retain some nucleophilic character (in the absence of fluoride) after alkoxide formation. Thus, we believe that the effect of increasing levels of fluoride incorporation is to diminish the nucleophilicity of these sites, thereby hampering ether formation. This effect is clearly different from the effects derived from simple site blocking, and we again cite our XRD and NMR evidence suggesting the formation of $(NH_4)_3AlF_6$ and AlF_3 at these higher loading levels; clearly the latter constitutes a source of appreciable Lewis acidity. These observations are also consistent with the observed ether desorption temperatures, which increase with added fluoride until 5 wt%, at which point they level off or decrease slightly.

Similar effects can be noted from a comparison of the ether/alkene ratios as a function of fluoride content (Table 3). Here we observe that these ratios increase on going from 0 wt% to 2 wt% fluoride, then begin to decrease above this fluoride level. Again, the latter is easy to understand on the basis of alkoxide proximity; as the fluoride levels increase to ca. 5 wt%, bulk AlF_2OH and AlF_3 are formed which serve to lower the surface alkoxide population and increase the mean inter-alkoxide separation. However, the initial step to 2 wt% fluoride results in a relative decrease in alkene production (relative to ether production); this is surprising since the electronegativity of the surface-bound fluorides would be expected to strengthen the neighboring Al-OR bond, thus facilitating O–R cleavage and alkene formation. However, this argument neglects the requirement for a base in the elimination reaction leading to alkene (Scheme 3) (*27*). We suggest that the addition of low levels of fluoride inhibits the alkene-forming reaction by reducing the population of surface base sites needed for elimination (*49*).

One of the strengths of the ^{18}O-alcohol method is its ability to distinguish between Lewis and Brønsted sites. Indeed, even IR

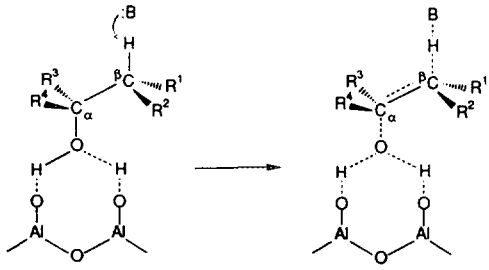

SCHEME 3. Mechanism for the base-catalyzed elimination reaction leading to alkene.

studies of adsorbed pyridine would be unable to distinguish between catalytically active surface Lewis acid sites and Lewis acidity due to the presence of crystalline or amorphous AlF_3 on the surface; it has also been noted that this method is quite sensitive to evacuation conditions, and that pyridine may be desorbed (*41*). On the basis of the results described herein, we can conclude that the effect of added fluoride is to *decrease* the number of Lewis sites while *increasing* the number of Brønsted sites; the latter effect is more prevalent than the former, so the composite trend is toward increased acidity. Nonetheless, it is important to be able to separate the two factors, and the new TPD method consitutes a useful complement to pyridine IR methods.

B. TPD results as a function of time. Alkene or ether desorption from Al_2O_3 may be induced 1 h or 1 week after the vapor deposition step with no apparent differences in the TPD data (*27*). Similarly, there are only minor differences in the partial ion chromatograms for the $F(2)/Al_2O_3$ sample over this time period. However, at higher fluoride loadings ($\geq 5\%$) the samples exhibit substantial differences upon standing in closed containers. This is illustrated in Fig. 14, which contains partial ion chromatograms for the production of $R^{16}OR$ (m/z = 59, 74) and $R^{18}OR$ (m/z = 61, 76) from the $F(5)/Al_2O_3$ sample. The data show that the production of $R^{18}OR$ is largely unaffected by the length of the interval, since there is no obvious change in desorption temperature and relatively little loss in signal area. In contrast, the production of $R^{16}OR$ is decidedly affected; in the first four hours there is little change in peak area, but a clear shift toward lower desorption temperature. Over the course of a week at room temperature, we observed nearly total loss of the species responsible for $R^{16}OR$ formation. Over the same time interval, the amount of alkene obtained was seen to diminish to one-sixth of its original value. These observations serve to illustrate three important points related to the behavior of alkoxides on the surface of fluorided alumina. First, they show conclusively that the ^{16}O-alkoxides and ^{18}O-alkoxides are *formed* at different sites and *remain* different over time; this is consistent with results we obtained previously for alumina (*27*). Second, the comparison between $R^{16}OR$ formation and al-

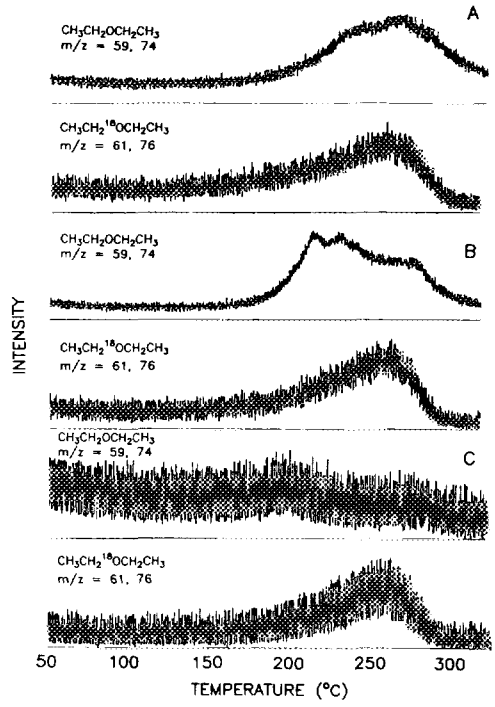

FIG. 14. Reconstructed partial chromatogram of the m/z = 59, 74 and m/z = 61, 76 signals for the $F(5)/Al_2O_3$ sample. (A) 1 h, (B) 4 h, and (c) 1 week, after the deposition of the ethanol-^{18}O.

kene formation suggests that alkene can arise from either ^{16}O-alkoxides or ^{18}O-alkoxides. The total loss of the former causes a concomitant six-fold decrease in alkene formation, but does not halt it entirely; indeed, alkene still represents the major elimination product. Finally, the TPD data show that ^{16}O-alkoxide sites are changing in character over time. The initial shift toward lower desorption temperature and the ultimate loss of all R^{16}OR-forming species suggests that the changes result in greater ease in elimination; since the sites were initially basic in character (*27*), we suggest that they are acquiring increasing acidic character over time. Since this behavior is not observed in the absence of appreciable fluoride levels, it appears that changes in the ^{16}O-alkoxide sites arise from the migration of AlF_2OH or AlF_3 toward those sites; this is entirely in accord with our XRD and NMR results, which suggest that these species are present in significant amounts only at fluoride levels $\geq 5\%$.

CONCLUSIONS

The work described in this paper shows that use of a combination of solid-state ^{27}Al NMR, FT-IR, and ethanol–^{18}O TPD techniques to study fluorided alumina samples can provide very useful information concerning the structure and acid–base properties of the catalyst surface. We have observed several competing trends resulting from the incorporation of fluoride, and some of our important conclusions are listed below:

(a) Solid-state ^{27}Al NMR is particularly sensitive to amorphous phases or small crystallites present on the catalyst surface, many of which cannot be detected by XRD. We have confirmed the presence of three types of $AlF_3(H_2O)_n$ species (with n varying between 0 and 3) on fluorided alumina, and used the MAS-NMR signals to reach conclusions regarding the symmetries of the aluminum ions contained therein.

(b) FT-IR studies of ethanol adsorption on F/Al_2O_3 samples show that fluoride promotes the associative chemisorption of ethanol at the expense of dissociative chemisorption. Additionally, it is observed that increasing the fluoride loading results in a decrease in the total number of alcohol molecules undergoing adsorption.

(c) FT-IR studies of pyridine adsorption indicate that there is an increase in the number of Brønsted acid sites with the addition of up to 10 wt% fluoride. However, increasing the fluoride loading to 20 wt% causes the number of Brønsted acid sites to decrease.

(d) The temperature-programmed desorption of ethanol–^{18}O from F/Al_2O_3 samples shows that incorporation of fluoride results in competing trends as a function of fluoride load level; at low levels fluoride serves to block Lewis acid sites, but at higher levels its predominant role is to increase the Brønsted acidity of the alumina surface. The addition of fluoride also decreases the nucleophilicity of the surface oxides.

(e) The ethanol–^{18}O TPD studies also demonstrate that alcohol is incorporated at different sites on alumina, tentatively identified as either Lewis acid or nucleophilic in character, and that the resulting alkoxides remain chemically distinct over a period of one week at room temperature.

(f) Alkene can arise from elimination at either type of alkoxide site provided the surface alkoxide population is diminished to a level at which bimolecular ether elimination is sufficiently hampered.

We are currently extending the use of the techniques utilized herein to the study of other promoted catalyst systems.

REFERENCES

1. Corbett, R. A., *Oil Gas J.* **June 18,** 33 (1990).
2. Choudhury, V. R., *Ind. Eng. Chem. Prod. Res. Dev.* **16,** 12 (1977).
3. Ghosh, A. K., and Kydd, R. A., *Catal. Rev.-Sci. Eng.* **27**(4), 539 (1985).
4. Moerkerken, A., Behr, B., Noordeloos-Maas, M. A., and Boelhouwer, C., *J. Catal.* **24,** 177 (1972).
5. Gerberich, H. R., Lutinski, F. E., and Hall, W. K., *J. Catal.* **6,** 209 (1966).

6. Finch, J. N. and Clark, A., *J. Catal.* **19,** 292 (1970).
7. Damon, J. P., Bonnier, J. M., and Delmon, B., *Bull. Soc. Chim. Fr.*, 449 (1975).
8. Allenger, V. M., McLean, D. D., and Ternan, M., *J. Catal.* **131,** 305 (1991).
9. Kordulis, C., Gouromihou, A., Lycourghiotis, A., Papadopoulou, C., and Matralis, H. K., *Appl. Catal.* **61,** 39 (1990).
10. Lewis, J. M., Kydd, R. A., and Boorman, P. M., *J. Catal.* **120,** 413 (1989).
11. Boorman, P. M., Chong, K., Kydd, R. A., and Lewis, J. M., *J. Catal.* **128,** 537 (1991).
12. Webb, A. N., *Ind. Eng. Chem.*, 261 (1956).
13. Sockart, P. O., and Rouxhet, P. G., *J. Colloid Interface Sci.* **86,** 96 (1982).
14. Tanabe, K., "Solid Acids and Bases." Academic Press, New York, 1970.
15. Kung, M. C., and Kung, H. H., *Catal. Rev.-Sci. Eng.* **27,** 425 (1985).
16. Tanabe, K., *in* "Catalysis by Acids and Bases" (B. Imelik, C. Naccache, G. Coudurier, Y. Ben Taarit, and J. C. Vedrin, Eds.), Vol. 20, p. 1. Elsevier, Amsterdam, 1985.
17. Benesi, H. A. and Winquist, B. H. C., *in* "Advances in Catalysis" (D. D. Ely, H. Pines, and P. B. Weisz, Eds.), Vol. 27. Academic Press, New York, 1978.
18. Tanabe, K., Misono, M., Ono, Y. and Hattori, H., "New Solid Acids and Bases," Vol. 51. Elsevier, Amsterdam, 1989.
19. McVicker, G. B., Kim, C. J., and Eggert, J. J., *J. Catal.* **80,** 315 (1983).
20. Kowalak, S., *Acta. Chim. Acad. Sci. Hung.* **107,** 27 (1981).
21. Kowalak, S., *Acta. Chim. Acad. Sci. Hung.* **107,** 19 (1981).
22. Hedge, R. I., and Barteau, M. A., *J. Catal.* **120,** 387 (1989).
23. Reitsma, H. J., and Boelhouwer, C., *J. Catal.* **33,** 39 (1974).
24. Scokart, P. O., Selim, S. A., Damon, J. P., and Rouxhet, P. G., *J. Colloid Interface Sci.* **70,** 209 (1979).
25. O'Reilly, D. E., *Adv. Catal.* **12,** 66 (1960).
26. DeCanio, E. C., Edwards, J. C., Scalzo, T. R., Storm, D. A., and Bruno, J. W., *J. Catal.* **132,** 498 (1991).
27. DeCanio, E. C., Nero, V. P. and Bruno, J. W., *J. Catal.*, in press.
28. Wade, K., and Banister, A. J., *in* "Comprehensive Inorganic Chemistry" (J. C. Bailar, H. J. Emeleus, R. Nyholm, and A. F. Trotman-Dickenson, Eds.), Vol. 1, p. 1012. Pergamon, Elmsford, NY, 1973.
29. Ketelaar, J. A. A., *Z. Kristallogr. Kristallgeom.* **85,** 119 (1933).
30. Akitt, J. W., *in* "Multinuclear NMR" (J. Mason, Ed.), p. 278. Plenum Press, New York, 1987.
31. Huggins, B. A., and Ellis, P. D., *J. Am. Chem. Soc.* **114,** 2098 (1992).
32. Kerkhof, F. P. J. M., Oudejans, J. C., Moulijn, J. A., and Matulewiez, E. R. A., *J. Colloid Interface Sci.* **77,** 120 (1980).
33. Bulgakov, O. V., and Antipina, T. V., *Russ. J. Phys. Chem.* **41,** 1680 (1967).
34. Morris, H. D., and Ellis, P. D., *J. Am. Chem. Soc.* **111,** 6045 (1989).
35. Knözinger, H., and Ratnasamy, P., *Catal. Rev.-Sci. Eng.* **17,** 3731 (1978).
36. Peri, J. B., *J. Phys. Chem.* **69,** 211 (1965).
37. Peri, J. B., *J. Phys. Chem.* **72,** 2917 (1968).
38. Peri, J. B., *J. Phys. Chem.* **70,** 3168 (1966).
39. Parry, E. P., *J. Catal.* **2,** 371 (1963).
40. Little, L. H., "Infrared Spectra of Adsorbed Species." Academic Press, New York, 1966.
41. (a) Morterra, C., and Cerrato, G., *Langmuir* **6,** 1811 (1990); (b) Kiviat, F. E., and Petrakis, L., *J. Phys. Chem.* **77,** 1232 (1973).
42. Haaland, D. M., *Surf. Sci.* **102,** 405 (1981).
43. Herzberg, G., "Infrared and Raman Spectra." Van Nostrand–Reinhold, New York, 1945.
44. Colthup, N. B., Daly, L. H., and Wiberley, S. E., "Introduction to Infrared and Raman Spectroscopy." Academic Press, New York, 1964.
45. Jeziorowski, H., Knözinger, H., Meye, W., and Müller, H. D., *J. Chem. Soc. Faraday Trans. 1* **69,** 1744 (1973).
46. Knözinger, H., and Stübner, B., *J. Phys. Chem.* **82,** 1526 (1978).
47. Lavalley, J. C., Caillod, J., and Travert, J., *J. Phys. Chem.* **84,** 2084 (1980).
48. Travert, J., Saur, O., Benaissa, M., Lamotte, J., and Lavalley, J. C., *in* "Vibration at Surfaces" (R. Caudano, J. M. Gilles, and A. A. Lucas, Eds.), p. 333. Plenum, Namur, 1982.
49. Peng, X. D., and Barteau, M. A., *Langmuir* **7,** 1426 (1991).